Global J. Environ. Sci. Manage. 9(2): 211-226, Spring 2023, Serial #34

Global Journal of Environmental Science and Management
(GJESM)

Homepage: https://www.gjesm.net/

Podcasts

ORIGINAL RESEARCH ARTICLE

Environmental vulnerability characteristics in an active swarm region

A.V.H. Simanjuntak[1,2,3], U. Muksin[3], A. Arifullah[3], K. Lythgoe[4], Y. Asnawi[5], M. Sinambela[6], S. Rizal[7], S. Wei[4,8]

[1] *Graduate School of Mathematics and Applied Sciences, Universitas Syiah Kuala, Banda Aceh, Indonesia*

[2] *Meteorological, Climatological, and Geophysical Agency, BMKG, Banda Aceh, Aceh, Indonesia*

[3] *Tsunami and Disaster Mitigation Research Center, Universitas Syiah Kuala, Gampong Pie, Indonesia*

[4] *Earth Observatory of Singapore, Nanyang Techonological of Singapore, Singapore*

[5] *Department of Science and Technology, Universitas Islam Negeri Ar-Raniry, Kopelma Darussalam, Banda Aceh, Indonesia*

[6] *Meteorological, Climatological, and Geophysical Agency, BMKG, Medan, Indonesia*

[7] *Graduate School of Mathematics and Applied Sciences, Universitas Syiah Kuala, Banda Aceh Indonesia*

[8] *Asian School of the Environment, Nanyang Technological University of Singapore*

ARTICLE INFO

Article History:
Received 28 June 2022
Revised 07 September 2022
Accepted 21 October 2022

Keywords:
Earthquake
Seismic
Spectral waveform
Swarm
Volcanic
Vulnerability

DOI: 10.22034/gjesm.2023.02.03

ABSTRACT

BACKGROUND AND OBJECTIVES: For the first time, an earthquake swarm occurred from April to August 2021 in Lake Toba (Indonesia), the world's largest caldera lake. Although the earthquakes were located in a volcanic environment, the swarm activities could also be related to tectonic activities on the Sumatran fault. The swarm activities occurred at shallow depths and may influence the ground surface condition in which soil or rock below the subsurface can amplify the shaking. The research objective was to investigate the characteristics of the earthquake swarm in the Toba Caldera from the spectrum of the earthquake waveforms, site frequency, and horizontal-to-vertical ratio of sites.

METHODS: The spectra of very closely located swarm and nonswarm earthquakes were analyzed to investigate the differences between both types of seismic events. The seismic spectral ratio of horizontal-over-vertical components was applied to calculate the spectrum in the active swarm region from all newly installed seismic sensors. The root mean square was applied to average the amplitude of the horizontal components. Then, the values of the horizontal-to-vertical ratios were obtained by comparing the average values of the horizontal and vertical components.

FINDINGS: The microtremor study showed a more complete spectrum waveform from the low-to-high frequency of a non swarm earthquake, while the swarm earthquakes generated high-frequency seismograms. From the combination values of natural site frequencies and the horizontal-to-vertical ratios, the Toba environment can be classified into five clusters: I) Samosir–Hasinggaan, II) Samosir–Parapat, III) Silimapuluh, IV) Balige–Paropo, and V) Panjaitan. Samosir Island located in the middle of the Toba Caldera has the highest frequency and amplification, which are divided into two clusters.

CONCLUSION: Cluster I, with high amplification corresponding to the earthquake intensity, was felt by people in northern Samosir. Cluster II is located in the southern part of Samosir Island. Cluster III features moderate values of amplification and seismic vulnerability and therefore needs attention before future infrastructure development. Cluster IV, located in the southern and northern regions with high amplification and vulnerability, is associated with the Quaternary eruption. Cluster V, situated in northeastern Toba, has the lowest amplification and vulnerability compared to other clusters. The microtremor results provide good correlation with the geology in the volcanic environment of the Toba region.

NUMBER OF REFERENCES	NUMBER OF FIGURES	NUMBER OF TABLES
40	7	0

*Corresponding Author:
Email: *muksin.umar@unsyiah.ac.id*
Phone: +6281 26328 9103
ORCID: 0000-0001-7297-8065

Note: Discussion period for this manuscript open until July 1, 2023 on GJESM website at the "Show Article".

INTRODUCTION

From April to August 2021, the local population was surprised by swarm activity that occurred in Lake Toba and its surrounding regions, as shown in Fig. 1. This swarm activity raises the question of its cause. Swarm activity can be either related to the movement of magma or hydrothermal fluids in a volcanic environment (Hayashi and Morita 2003) or continuous slips along preexisting faults caused by stress changes (Gualandi *et al.* 2017). The cause of the Toba earthquake swarm remains unclear. A simple method for understanding the cause of an earthquake swarm is assessing and comparing the waveform spectra of swarm and nonswarm earthquakes. Understanding the cause of swarm earthquakes is important so that a population or government can take appropriate mitigating action to reduce the future possible risks. Meanwhile, the strong shaking of 2–3 MMI caused by an earthquake swarm with magnitude of M ~3.0 created public concern about potential damage to Lake Toba and its surroundings. Shaking can be also caused by nonswarm earthquakes, such as the 2004 Indian Ocean earthquake with an M of 9.0 and the 2005 Nias earthquake with an M of 8.5 that were strongly felt at Toba Lake, while inland destructive earthquakes emanate from the Sumatra fault system.

The inland earthquakes are distributed along the Sumatra fault system (Sieh and Natawidjaja 2000), including the Renun fault and the Toru fault as the closest active faults to the Toba region (Muksin *et al.,* 2013, 2014). Both faults have generated major earthquakes near the Toba region accompanied by massive damage (Pasari *et al.,* 2021). Several major earthquakes occurred along the Renun segment in 1916 and 1921 with M~7, while the Toru fault has not generated a major earthquake larger than M 6.5 (Muksin *et al.,* 2014; Hurukawa 2014). The largest earthquake from the Toru fault occurred in 1984 (M 6.4) and caused serious damage and loss in the city of Tarutung (Ryberg *et al*., 2016; Pasari *et al.,* 2021). The most recent earthquakes on the Toru fault occurred along the Sarulla Basin in 2008 (M 6), 2011 (M 5.5) (Muksin *et al.,* 2013) and 2020 (M 5.4). Further, several major earthquakes were also felt in Toba, such as the doublet earthquake in 1926 (M 6.5 and M 6.8) and 2007 (M~6) that occurred on the Suliki and Sumani fault segments (Daryono *et al.,* 2012). In the last decade, no major events have been recorded near Toba, but the swarm activities suggest the potential for an unknown local tectonic system inside Toba that can generate a strong shaking. Among the swarm events, three earthquakes (M~3) with an MMI of 2–3 were strongly felt by the local population but without severe damage. Therefore, mitigation plans to anticipate either the volcanic or the tectonic impact in Toba should be prioritized because the region is highly populated and considered the most popular tourist destination in Sumatra. Several studies have been undertaken to highlight the environmental condition of Toba, involving geological modeling (Chesner *et al.,* 2008), tomography imaging (Koulakov *et al.,* 2010; Koulakov *et al.,* 2016), water pollution (Soeprobowati 2015), and the impact of climate change on the water level in Toba (Irwandi *et al.,* 2021). Although the Toba region is seismically active from tectonic and (possible) volcanic activities, no study has been conducted on its environmental vulnerability, particularly to seismic activities and microzonation. In May 2021, a seismic survey was conducted to assess the seismic amplification and the vulnerability level of Lake Toba. Seismic records can be used to study the horizontal-to-vertical spectral ratio (HVSR) and natural frequency based on microtremor data to derive the seismic vulnerability of the Toba region. Microtremor HVSR has been widely applied to assess the potential damage caused by earthquakes by using specific parameters such as seismic amplification and natural frequency that relate to the geological condition (Goda *et al.,* 2015; Parker *et al.,* 2015). Locations with possible damage during earthquakes are categorized as areas with low dominant frequencies (Nakamura 2009). Microtremor HVSR is one of the least expensive methods and is easy to operate where areas are inaccessible. The HVSR result is recommended for soon assessing a detailed soil cluster and its projected effect. Furthermore, the results can also be used to study the probabilistic seismic hazards to help diminish the potential losses in Toba. This study aims to investigate the vulnerability after swarm phenomena in a specific cluster in Toba. Another research objective is to define the possible cause of the swarm earthquake from different swarm and nonswarm earthquake spectra recorded by the same seismic stations. This seismic experiment was performed in Toba and its surroundings in Indonesia from April to May 2021.

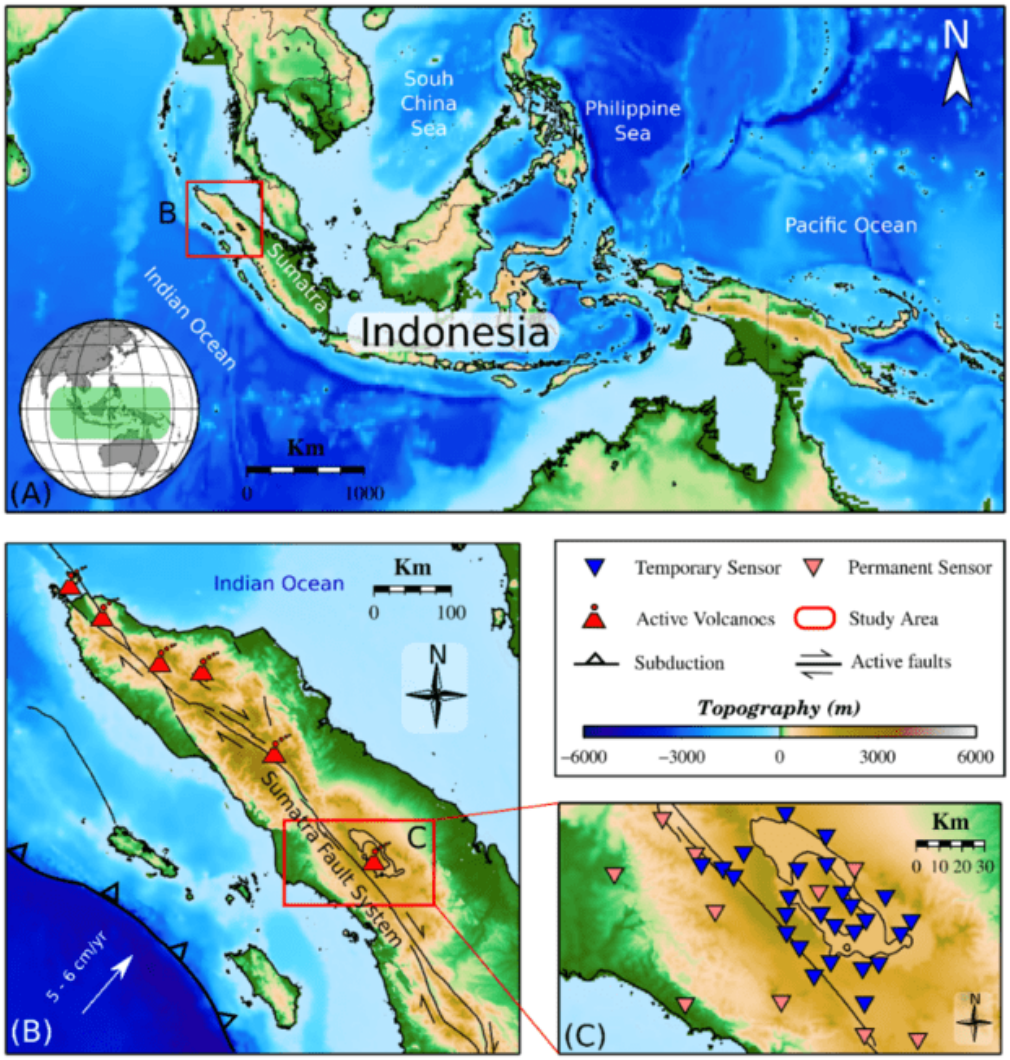

Fig. 1: (a) Geographical map of Indonesia and the study area in the northernmost part of Sumatra. (b) The tectonic map of the northernmost part of Sumatra features active subduction with a geodetic slip rate of 5–6 cm/yr and the Sumatra fault system with active volcanoes. The red square is the boundary area located in Lake Toba and its surroundings. (c) The study area in Lake Toba and its surroundings and the observation points from a temporary sensor (blue triangle) and a permanent sensor (red triangle).

Geology of the study area

Caused by a supereruption 74,000 yr B.P., the Toba caldera is one of Earth's many complex volcanic systems. The Toba volcano has erupted four times since the Quarternary, making a large depression area in northern Sumatra (Chesner *et al.,* 1991; Geethanjali *et al.,* 2019; Chesner *et al.,* 2020). As aforementioned, it is the largest of calderas, and the current condition of the complex volcanic system is influenced by the youngest Toba eruption that removed 2,800 km^3 of dense-rock-equivalent of rhyolitic magma at 74,000 yr B.P. (Chesner *et al.,* 2020; Pearce *et al.,* 2020). The young Toba tuff (YTT) (Fig. 2) was formed during the last eruption of the Toba volcano in the Late Pleistocene as a large area comprising pyroclastic material (Chesner and Luhr 2010; Chesner 2012). Eruption ash is detected at many locations in South Asia by paleoclimate studies, with

the results indicating an escalation of eruptions. The ash is composed of middle Toba tuff (MTT) (504 ka), old Toba tuff (OTT) (840 ka), and Haranggaol Dacite tuff (1.2 Ma) (Knight *et al.,* 1986; Chesner *et al.,* 1991) from previous eruptions. The YTT eruption removed a global mass of ash and various gases (Sarma *et al.,* 2018) that make a paleoclimate phenomenon with acid rain (Chesner and Luhr, 2010), resulting in the devastation of vegetation and living populations (Pearce *et al.,* 2020).

Geologically, the Toba tuff has special characteristics comprising the subsurface condition with low seismic velocity (Vs). Stankiewicz *et al.* (2010) found low Vs surrounding the Toba caldera. Low Vs can be associated with the presence of a magma chamber beneath the caldera, while at shallow depths, low Vs can be also interpreted as soft soil or rock (Asnawi et al., 2022) compared to the surrounding region. A low Vs value can also cause high seismic amplification and is subsequently classified as high seismic vulnerability. Therefore, an investigation of seismic amplification and vulnerability in the Toba region is considered essential.

MATERIALS AND METHODS

Microtremor acquisition

Microtremors were measured using two types of seismometers. The first type was a portable nodal seismic sensor used to record microtremors at 27 sites, and the second type was a broadband permanent seismic sensor used to record 9 sites (Fig. 2). The portable seismic sensor with a Magseis Fairfield nodal array was applied using three geographical components with a corner frequency of 5 Hz, a 24-bit ADC, and the ability to record with a 200 sps continuous reading. The observation location was set by a grid space of 10–30 km depending on the access to the site, with the recording time length at each site set at 45–60 min. The permanent station was equipped with a Nanometrics broadband seismometer with a sensitivity of 750 V/m ± 0.5% and operated by the Meteorology, Climatology, and Geophysics Agency (BMKG, Indonesia) to record the seismic activities in Sumatra. The sampling rate from the permanent seismic station was set to 40 sps with an effective resolution of 22 bits. The recording data of the portable and permanent seismic sensors were gathered at night to reduce the transient noise from human and machine activities. The seismic waveform was then used to calculate parameters such as the amplification and dominant frequency and subsequently to derive the seismic vulnerability.

HVSR microtremor processing

The HVSR is globally applied to assess the vulnerability level of a seismically active environment. Nakamura (2009) first developed the method with a single seismic sensor. The amplitude in the vertical shaking value is normally stable, while the amplitude in the horizontal direction is dominantly influenced by the soil subsurface condition that may receive a substantial amplification effect (Nakamura, 2009). Assuming the H/V as the frequency function that corresponds to the site characteristic, Nakamura (2009) found that the local effect can be measured using the spectral ratio of horizontal-over-vertical components using Eq. 1 (Nakamura, 2009).

$$\frac{H}{V} = \frac{\sqrt{NS^2 + EW^2}}{V} \quad (1)$$

The root mean square was applied to average the NS and EW as the representative of the horizontal components. The average of the horizontal amplitude was divided by the vertical amplitude to obtain the average H/V spectrum. From the H/V spectrum, the dominant frequency and period can be obtained at the H/V peak, which is associated with seismic amplification. The dominant frequency is closely related to the lithological conditions and thickness of the subsurface. The H/V spectrum is related to the rock density. The amplification value is large for areas composed of low-density rocks or soil. Seismic surface waves propagate slowly in soft sediments, and ground shaking can be amplified and thereby cause severe damage. The seismic vulnerability index (K_g) is calculated by dividing the square of the amplification with the dominant frequency using Eq. 2 (Nakamura, 2009).

$$K_g = \frac{A^2}{F} \quad (2)$$

The K_g value can be used to categorize the subsurface soil and qualitatively estimate possible damage areas (Tün *et al.,* 2016; Seivane *et al.,* 2022). Some studies have applied the result of K_g to assess an earthquake-prone area for earthquake mitigation

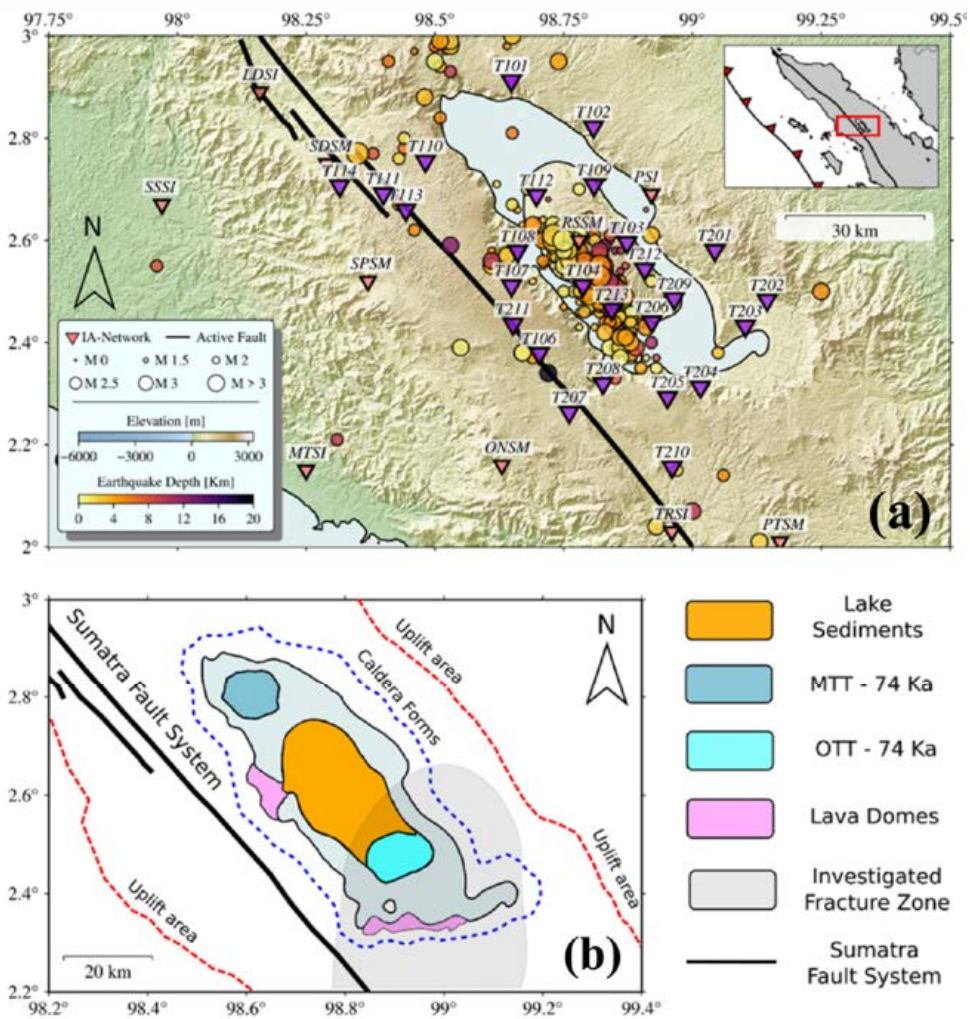

Fig. 2: (a) The seismicity map of the Toba area maps the swarm activities mostly located at Samosir Island and distributed in the NW–SE direction parallel with the Sumatra fault system (Chesner 2012). The seismometer for recording the seismic waveforms is divided into two types, temporary (purple triangle) and permanent (red triangle). (b) The local geological map of Toba features the lake sediments as the dominant geological unit. The three eruptions make a different rock age with old Toba tuffs (OTT)—840 ka, middle Toba tuffs (MTT)—500 ka, and young Toba tuffs (YTT)—74 ka.

plans (Boore 2004; Claprood *et al.,* 2014; Manzo *et al.,* 2022; Jiang *et al.,* 2022). This study is the first on seismic vulnerability based on swarm earthquakes in the Toba region.

RESULTS AND DISCUSSION

Example results of microtremor processing are shown in Fig. 3. A band pass filter with a range of 0.1–10 Hz was applied to the seismic waveform. The filtered waveform was segmented into several specific windows, as shown in Fig. 3a, and then a fast Fourier transform was applied to all accepted windows to transform the time domain data into the frequency domain (spectra). An STA/LTA antitriggering with a threshold range of 0.1–0.5 s was applied to exclude the transient noise from further analysis. After the transient effect was reduced, a 5% cosine taper was used to improve the spectrum quality of the frequency domain.

The examples of waveforms with spectrograms

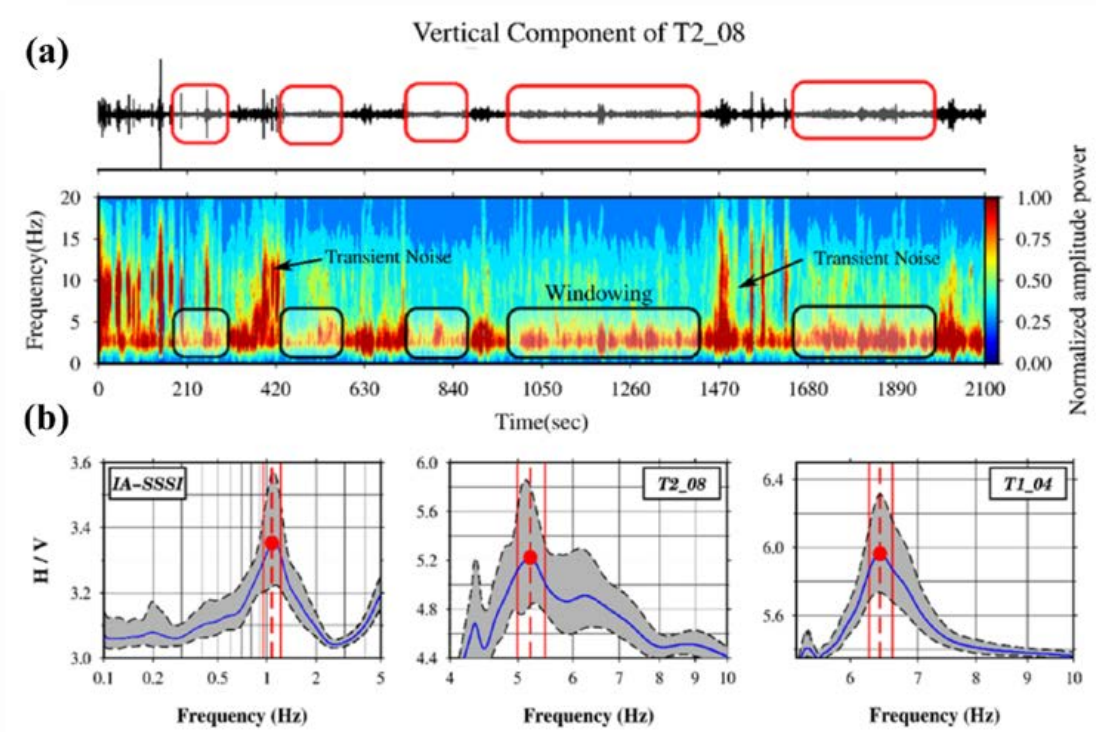

Fig. 3: (a) Example recording of the vertical component in 2100 s at site T208 and the spectrogram with a frequency range of 0–20 Hz. (b) The selected windowing is marked by a frequency of <5 Hz, while the transient noise is marked by a sudden peak. (b) Example of the H/V graph results from IA-SSSI as the permanent sensor and T2_08 and T1_04 as the temporary sensor.

(Fig. 3) show the quality of the seismic records. The selected waveform ranged from 1 to 5 Hz, while the transient noise shows a sudden peak in the high-frequency range. The three example results (IA-SSSI in the eastern part of the study area and T2_08 and T1_04 at Samosir Island) show different characters of subsurface soil response. The different H/V values for the three locations indicate variations in the site conditions depending on the rock properties of the area.

Analysis of swarm and non-swarm earthquakes

To propose the correct mitigation action, the cause of the earthquake swarm either by volcanic or tectonic activities must be investigated, which is undertaken by examining the spectra of swarm and nonswarm earthquake ash shown in Fig. 4. The chosen earthquakes occurred at different times but were located near each other. These swarm and nonswarm earthquakes were recorded by the same station and then the spectrum characteristics of the seismic waveforms from both earthquakes were analyzed.

The swarm recording shows high-frequency content larger than 10 Hz, which may be associated with possible hydrothermal fluid migration (Horton, 2012; Ross and Cochran, 2021). An earthquake swarm can also occur along the preexisting fault triggered by stress changes, caused by dike intrusion from the upper-crust layer. From the distinction of waveform frequencies, the cause of the intensity felt from the earthquake swarm in Toba was assumed to be a possible large sediment layer beneath the subsurface. A similar study determined the high-frequency content from a fluid-driven earthquake swarm in a Yellowstone caldera lake (Shelly *et al.*, 2013). Based on that study, the comparisons from some stations must be manually checked, as shown in Fig. 5.

The example recordings from different stations show the possible amplification effect beneath sensors T110 and T203. The waveforms from both

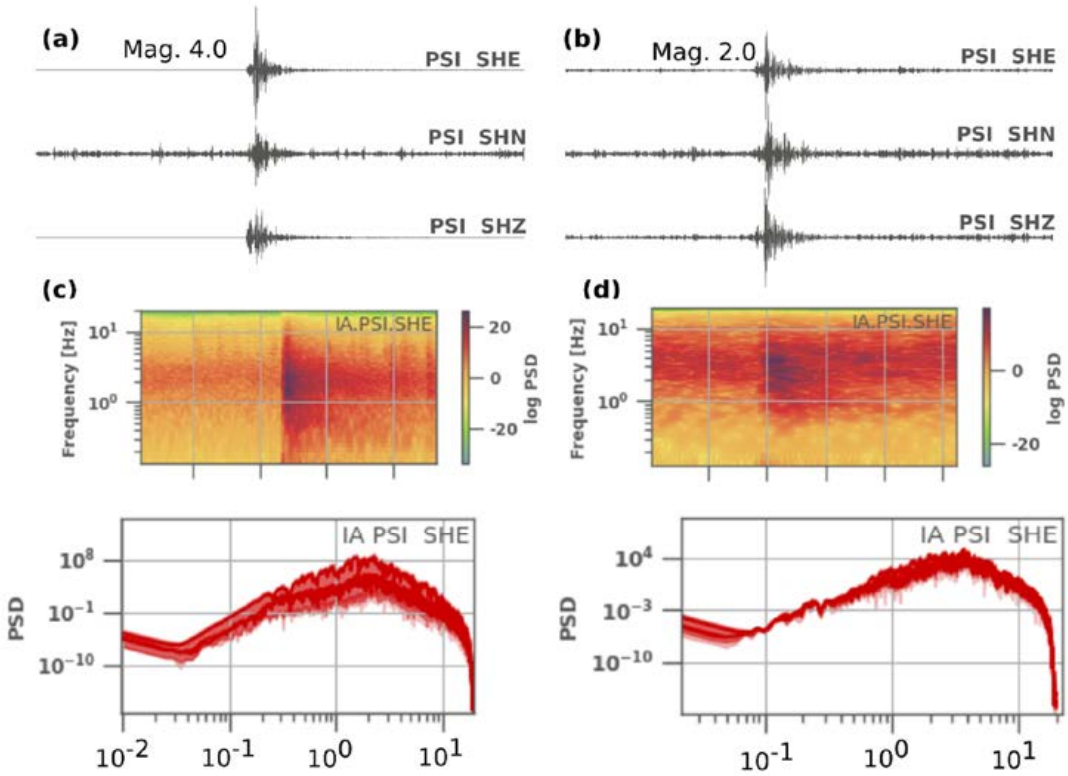

Fig. 4: (a) Example recordings of nonswarm and (b) swarm earthquakes. (c) Example spectrograms and power spectral densities (PSDs) of nonswarm (BOTTOM LEF and swarm (BOTTOM RIGHT) earthquakes. The spectrogram shows that the swarm earthquake has more high-frequency content than the nonswarm earthquake.

stations show a noise artifact that can be associated with the subsurface sediment. The spectrogram from four stations also shows T110 and T203 with saturated PSD influenced by the sediment subsurface. All sensors were manually inspected to assess the waveform quality that can be used to measure the possible site effect and support the separation of clusters based on the H/V value in the study area. The waveform spectrum of the swarm earthquake recorded by some stations in Fig. 5 follows the characteristics of the natural frequency recorded at each site. The natural frequency and H/V value at each measurement point having been obtained, the effect of the swarm earthquake in the study area can be investigated as the environmental conditions supporting soil or rock. In general, stations located in a region with high H/V will record high amplitude at the natural frequency.

Interpretation of HVSR results

After all results were collected, the microtremor parameters such as frequency and amplification were compiled to interpret the condition of the subsurface soil in the study area. The maps of the parameters of dominant frequency and period, the H/V values, and the vulnerability index are provided in Fig. 6. High dominant frequencies were recorded in Samosir Island, while low frequencies were located in the northern and southern parts outside Toba Lake (Fig. 6). In contrast to dominant frequencies, low dominant periods were observed along the Sumatra faults and outside Samosir Island (Fig. 6). The amplification obtained from the vertical axis of the peak of the H/V curve shows the highest amplification in Samosir Island, which can be related to the earthquake intensity felt by the local population (Maresca *et al.,* 2018; Alamri *et al.,* 2020).

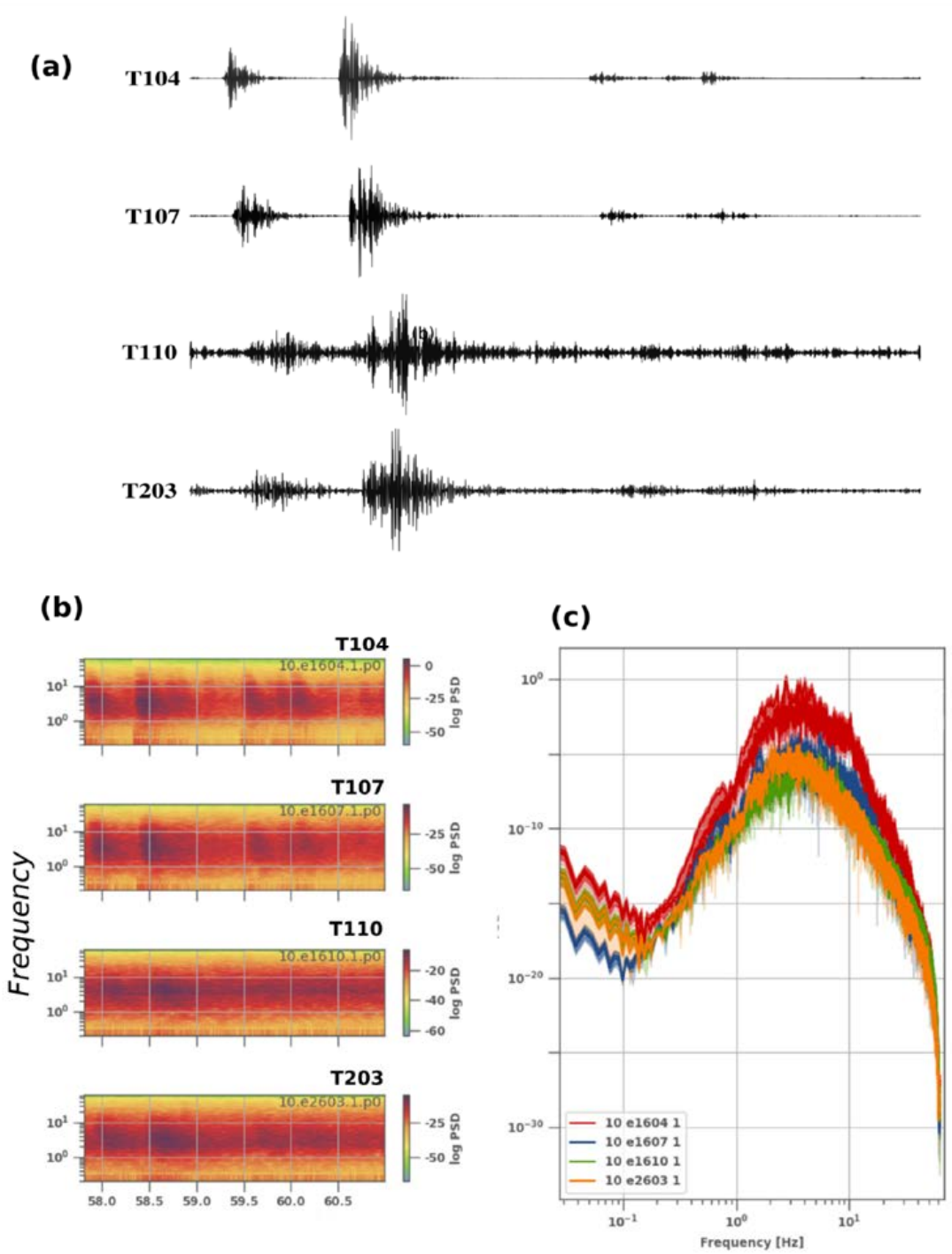

Fig. 5: (a) Example recording of two swarm events in the four sensors. The T110 and T203 stations show noise artifacts that can be associated with the subsurface condition. (b) The spectrogram from four stations also shows T110 and T203 with saturated PSD that can be related to the sediment subsurface. (c) The Fourier transform graph from all recordings highlights that T104 and T107 have higher amplitude factors than T110 and T203 (c).

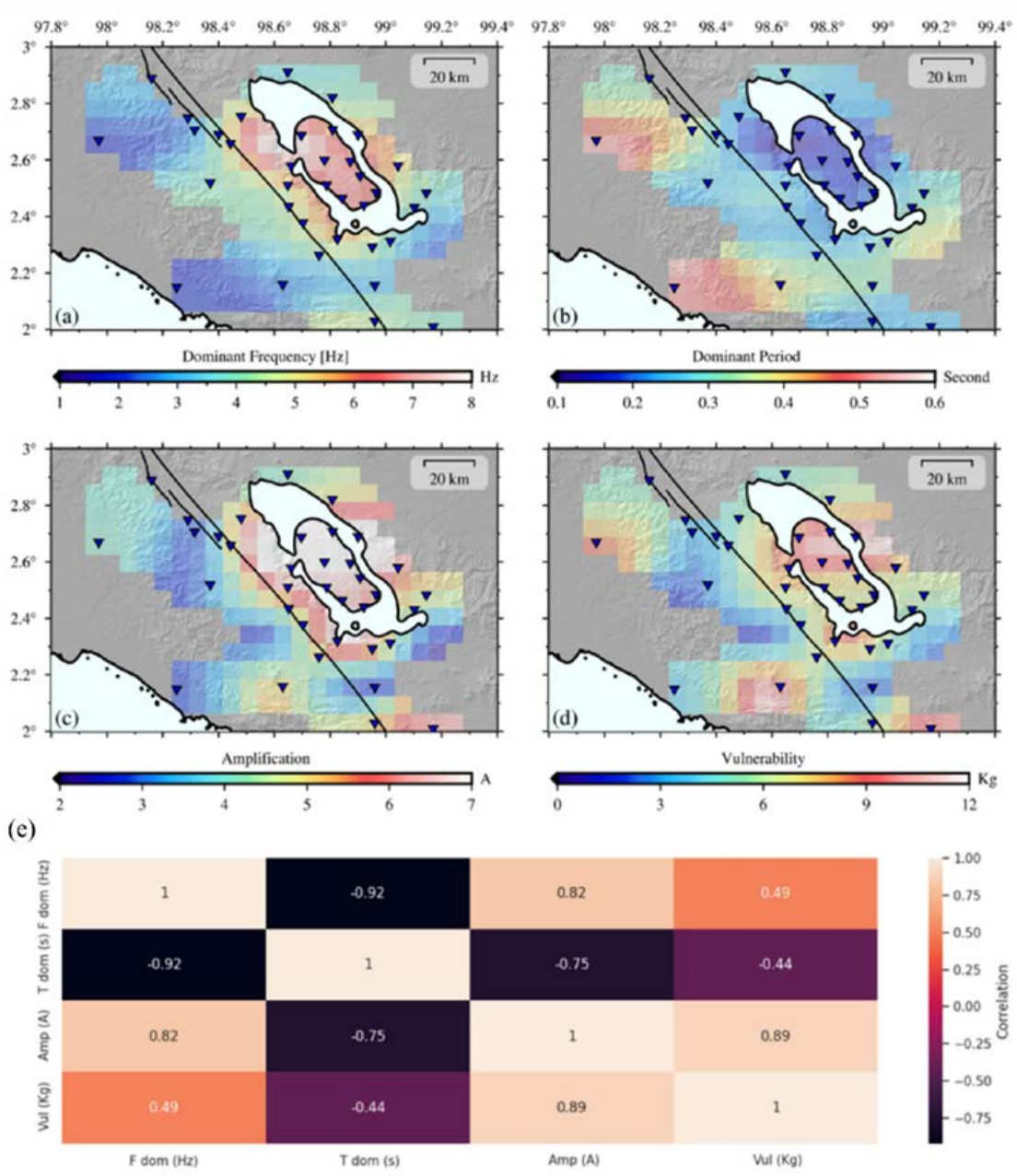

Fig. 6: (a) Spatial interpolation results of the HVSR result in dominant frequency, (b) dominant period, (c) amplification, and (d) vulnerability. (e) The heat map graphic explains the relationship between microtremor results and the correlation to all parameters.

Fig. 6(a – d) shows the map of dominant frequency and period as well as the seismic amplification and vulnerability. The seismic vulnerability K_g is highest mostly in the northern part of Samosir Island and lowest along the Renun segment of the Sumatra fault segmentation. Then, all seismic parameters, including dominant frequency, amplification, and seismic vulnerability, were spatially grouped into a specific

cluster. The relationship among all parameters (Fig. 6e) shows a linear correlation between amplification and vulnerability with a correlation value of 0.89 and amplification and frequency with a correlation value of 0.82. To examine the clusters, the seismic parameters were interpreted based on the geological condition and swarm zone mostly located in Samosir Island. Here, the low dominant frequency in the study area might be associated with the lithological condition that is composed of thick volcanic sediment layers in the upper subsurface, while the low frequency could be related to the solid rock structure. In general, the result of the dominant frequency due to the Rayleigh waves has a long period content that may connect with the lithological condition in which a thick layer lies beneath the sediments (Stanko *et al.* 2017; Forte *et al.* 2019). On the basis of the dominant frequency, the five clusters (Fig. 7) are Cluster I in northern Samosir Island and Hasinggaan, Cluster II in southern Samosir Island and Parapat, Cluster III in Silimapuluh, Cluster IV in Balige and Paropo, and Cluster V in Panjaitan.

Cluster I (Samosir Island - Hasinggaan)

Cluster I is located in northern Samosir Island and the Hasinggaan region (Fig. 7). Samosir Island is composed dominantly of lake sediment and therefore most stations recorded high amplification and frequency. The lake sediment may influence the amplification of the seismic waveform due to the

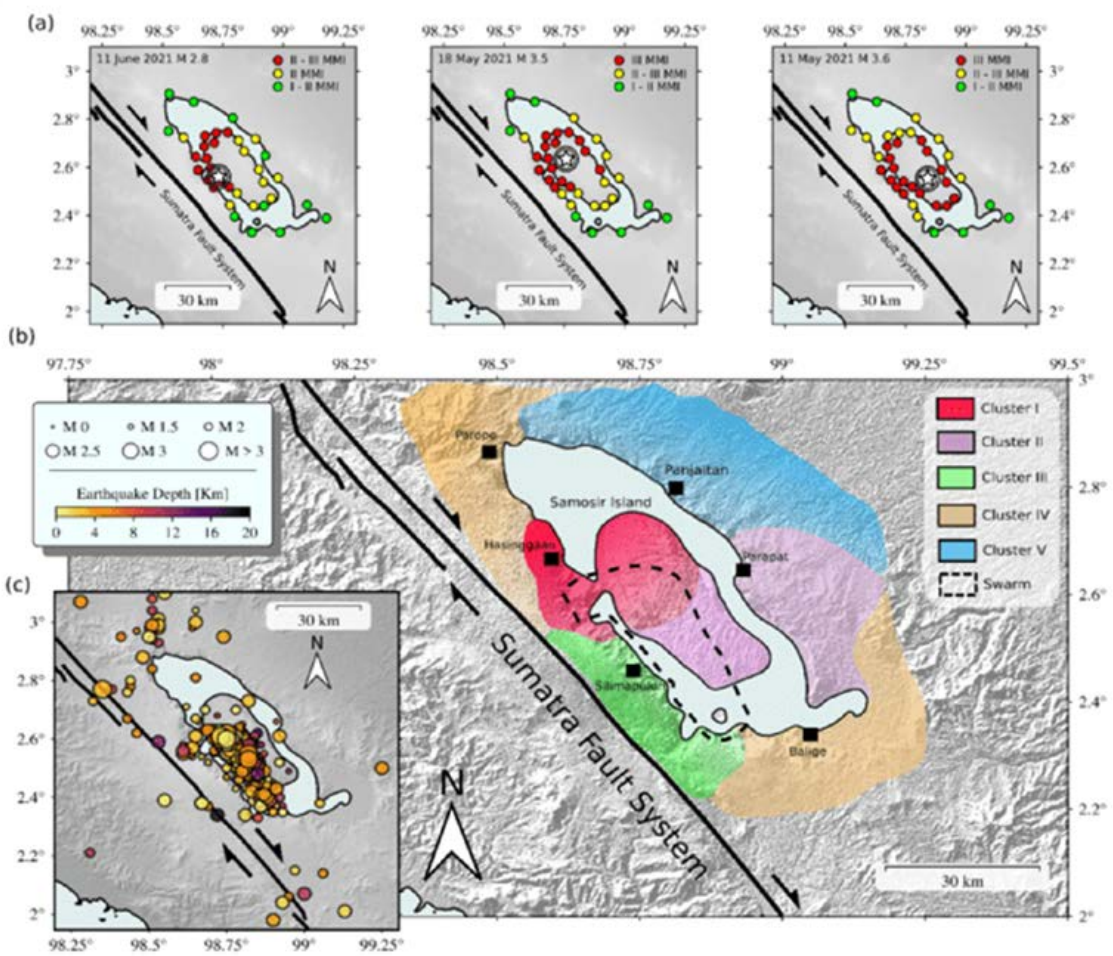

Fig. 7: (a) Clusters of zonation derived from the combination of dominant frequency and amplification (A) in the Toba area. (b) The area is divided into five clusters: Cluster I in northern Samosir Island and Hasinggaan, Cluster II in southern Samosir Island and Parapat, Cluster III in Silimapuluh, Cluster IV in Balige and Paropo, and Cluster V in Panjaitan. (c) Swarm earthquake location in the Toba area.

weak soil associated with volcanic deposits (Boore 2004; Claprood *et al.,* 2012). The amplification is relevant for the report on the earthquake felt by the local population in the central and northern parts of Samosir Island. Most people in the north of Samosir Island reported higher shaking compared with the southern part, as shown in Fig. 5(a). On the other hand, the dominant frequency ranges in Cluster I have the highest values, being between 7 and 8 Hz. The lake sediment is interpreted to have a thin layer, while the rock formation may have a thick layer below the subsurface. With the highest frequency and amplification parameters, Cluster I has a vulnerability value K_g of 9–12.

Cluster II (Samosir Island - Parapat)

Different subsurface soil characteristics divide Samosir Island into two clusters, Cluster I in the northern part and Cluster II in the southern part. The southern part of Samosir–Parapat has a slightly lower dominant frequency, with a range of 5–7 Hz. Geologically, the rock formation in the southern part of Lake Toba is older than that in the northern part, and it makes the sediment layer thicker. The OTT formation is the first quartz-bearing rock that was erupted, and this event created the Porsea caldera (Chesner *et al.* 2008). The deeper sediment layer makes a lower natural frequency range than the northern part. The Parapat region has lower seismic parameters, but both regions have similar values at the vulnerability level.

Cluster III (Silimapuluh)

The Silimapuluh region is categorized as Cluster III with a moderate amplification value and natural frequency. Cluster III is located in the southwestern part of YTT. The rock structure can be found along the Silimapuluh region. Cluster III has moderate parameters with a dominant frequency of 4–6 Hz, a dominant period of 0.2–0.3 s, an amplification of 5–6, and a seismic vulnerability K_g of 6–9. However, the moderate vulnerability level needs more attention due to the active fault in the western part. The right lateral Renun fault is suggested to have a slip rate of ~2 cm/yr. Furthermore, future studies must be conducted with more observation points in the western part of Cluster III and covering the Renun fault lineation to prepare a mitigation plan based on active faults near Toba.

Cluster IV (Paropo - Balige)

Cluster IV is located in the southern and northern parts of Lake Toba outside Samosir Island and is also constituted by OTT. The Quaternary eruption created the caldera in Balige. Cluster IV has a dominant frequency range of 3–4 Hz, the dominant period being ~0.3 s in Balige and ~0.4 s in Paropo, while the seismic amplification is less than 4 in Balige and greater than 4 in Paropo. The seismic vulnerability is classified as high with a seismic vulnerability K_g of 6–9 for the Balige and Paropo areas. Similar seismic parameters in the north and south indicate that the subsurface soil is mostly identical and the soil is formed by OTT from the Quaternary eruption. Cluster IV is located outside the swarm zone and Samosir Island, but it still needs a mitigation plan to reduce the effect of earthquake-derived shaking.

Cluster V (Panjaitan)

Cluster V is located in the northeastern part of Lake Toba, namely, in the Panjaitan region. Cluster V has a lower parameter than other clusters. The dominant frequency in the Panjaitan Cluster is 3–4 Hz, with an amplification of 5–6 and a seismic vulnerability K_g of 3–6. The population in the Panjaitan region did not report any shaking caused by the swarm earthquake because Panjaintan is far from the swarm center. The subsurface of Cluster V is mostly composed of YTT, as shown in the geological map (Fig. 2). On the basis of a lower frequency, the tuff deposit in Cluster V may indicate a larger layer in the upper subsurface compared to other clusters. However, Cluster V also needs a mitigation plan to anticipate the potential shaking derived from a swarm earthquake.

CONCLUSION

The swarm earthquake in the Toba region has changed the seismicity distribution that was distributed northwest–southeast in Samosir Island. The swarm earthquake can be considered an important event because of its shallow depth and repeated shaking duration of approximately 2–3 MMI. Therefore, a microtremor study was conducted to ascertain the previously unknown soil properties in Toba and the surrounding region. The novelty of five specific clusters was found based on the dominant frequency, seismic amplification, and vulnerability recorded by seismic temporary sensors. Cluster I is located in northern Samosir Island and in Hasinggaan

and is dominantly composed of lake sediment and characterized by high amplification and frequency. The amplification is relevant for the report about shaking felt by the local population in central and northern Samosir Island. The dominant frequency range in Cluster I has the highest values of 7–8 Hz from the lake sediment that may have a thin layer below the subsurface that produces the highest vulnerability index. The characteristics of Cluster II in southern Samosir Island are similar to those of Cluster I. The rock formation in the southern part of Lake Toba is older than that in the northern part, and it makes the sediment layer deeper. The range of the dominant frequency is lower in the southern part of Samosir Island than in the northern part, which correlates with the thicker sedimentary layer in the north. Cluster III (Silimapuluh) region has moderate amplification and vulnerability in the southwestern part of YTT and needs attention because of several major earthquakes in the last decade. Cluster IV is located in the southern and northern parts of Lake Toba and also the OTT location. The parameters in Cluster IV have a dominant frequency range of 3–4 Hz, a dominant period of ~0.3 s in Balige and ~0.4 s in Paropo, an amplification of <4 in Balige and >4 in Paropo, and K_g is 6–9 for both regions. Similar parameter values indicate the subsurface soil is mostly the same, which is formed by OTT from the Quaternary eruption. Cluster V is located in the northeastern part of Lake Toba, namely, in the Panjaitan region, and it has the lowest parameter. The dominant frequency is 3–4 Hz, the dominant period is <0.2 s, the amplification is 5–6, and K_g is 3–6. Cluster V is mostly composed of YTT as the subsurface soil, which has a lower frequency, indicating that the deposited layer may be larger in the upper subsurface. The clusters of the microtremor results provide a satisfactory spatial interpretation that is consistent with the recent geological condition and properties in the study area. A comprehensive study with more observation points with shear wave velocity must be conducted in the western part where the Sumatra fault is located. Further, this microtremor study in the swarm zone is the first research effort in the Toba region, which is important for reducing the environmental risk based on swarm earthquake disaster mitigation and policy.

AUTHOR CONTRIBUTIONS

A.V.H. Simanjuntak contributed by conducting the field experiments, HVSR data analysis, maps and figures production as well as interpreting the results, and drafting the manuscript. U. Muksin is the corresponding author and the leader of the project who provided funding for the project. A. Arifullah conducted the field experiments, and collected the seismic waveform data. Y. Asnawi was involved in data acquisition. K. Lythgoe supervised the field experiments, analyzed and interpreted the results. M. Sinambela conducted field experiments and the waveform data from BMKG. S. Rizal supervised the data processing and provided critical revision of the manuscript. S. Wei supervised the field experiments, analyzed and interpreted the results, and finalized the draft. All authors were involved in writing the manuscript.

ACKNOWLEDGEMENT

The microtremor experiment was conducted in Toba Lake, Northern Sumatra, Indonesia after swarm phenomena in 2021 by the team from Universitas Syiah Kuala (USK) and Meteorological, Climatological, and Geophysical Agency of Indonesia (BMKG). The seismic instruments were provided by Earth Observatory of Singapore of Nanyang Technological of Singapore (EOS – NTU). Authors thank to the additional waveform data from seismic station from Meteorological, Climatological, and Geophysical Agency of Indonesia (BMKG) in North Sumatra province. Authors also thank to the two anonymous reviewers for their fruitful comments and suggestions. The microtremor research was part of the World Class Research with the contract number [55/UN11.2.1/PT.01.03/DPRM2021].

CONFLICT OF INTEREST

The authors declare no potential conflict of interest regarding the publication of this work. In addition, the ethical issues including plagiarism, informed consent, misconduct, data fabrication and, or falsification, double publication and, or submission, and redundancy have been completely witnessed by the authors.

OPEN ACCESS

PUBLISHER'S NOTE

GJESM Publisher remains neutral with regard to jurisdictional claims in published maps and institutional affiliations.

ABBREVIATIONS

%	Percentage value
°C	Degree in Celsius
0°	Azimuth angle in 0 degree
1D	1-Dimension profile
A	Amplification
A	Amplitude
A^2	Square of the amplification
AB04	04th observation Point
AB05	05th observation Point
AB09	09th observation Point
AB13	13th observation Point
AB22	22th observation Point
AB23	23th observation Point
AB27	27th observation Point
b	Bandwidth coefficient
Bits	Bit per sample
B.P	Before Present
	Soil class for sediment – Rock
C-D	Line of cross section from C to D
cm	centimetre
cm/year	Centimetre over year
D	Soil class for sediment
E	Soil class for soft sediment
E-D	Soil class between soft sediment and hard soil
E-F	Line of cross section from E to F
e.g.	Latin phrase example gratia (for example)
Eq	Equation
EW	Spectrum amplitude in the horizontal east-west component
EW	East-west
f	Frequency
f	Dominant frequency
Fig.	Figure
H/V	The horizontal-to-vertical spectrum
H/V peak	Maximum peak of horizontal-to-vertical spectrum
HVSR	Horizontal to vertical spectral ratio
Hz	Hertz
i.e.	Latin phrase Id est (this is)
IA	Indonesia Seismic Network
IA-SSSI	Subulussalam Seismic Station Code
Idi	Idi Formation
Ka	Kilo annus (one thousand years)
K_g	Seismic vulnerability index
km	kilometre
km^3	cubic kilometre
log	logarithmic
m	meter
M	magnitude
m/s	meter per second
min.	minute
ms	millisecond
Ma	mega annum (5 million years from the present)
MMI	Modifie mercalli intensity

MTT	Middle Toba Tuff
NEHRP	National Earthquake Hazards Reduction Program
N	North Geographic
NS	Spectrum amplitude in the horizontal north–south component
NS	North-South
NW	North-West
OTT	Oldest Toba Tuff
PSD	Power Spectral Density
s	second
sps	Sampling per second
STA/LTA	Ratio between the amplitude
SW	South-West
T	Period
T1_06	Observation Point at T1_06
T1_09	Observation Point at T1_09
T2_08	Observation Point at T2_08
USD	United State Dollar
V	Spectrum amplitude in the vertical component of seismic waveform
V/m	Seismometer sensitivity (volt/meter)
Vp	Velocity of pressure
Vs	Shear Velocity
WCP	World Class Professor
Z	Vertical Component
YTT	Young Toba Tuff
π	Pi is a mathematical constant (3,14159)

REFERENCES

Alamri, A.M.; Bankher, A.; Abdelrahman, K.; El-Hadidy, M.; Zahran, H. (2020). Soil site characterization of Rabigh city, western Saudi Arabia coastal plain, using HVSR and HVSR inversion techniques. Arabian J. Geosci., 13(1): 1-16 **(16 pages).**

Asnawi, Y.; Simanjuntak, A.; Muksin, U.; Rizal, S.; Syukri, M.; Maisura, M., Rahmati, R. (2022). Analysis of Microtremor H/V Spectral Ratio and Public Perception for Disaster Mitigation. Geomate J., 23(97): 123-130 (**8 pages**).

Boore, D.M., (2004). Estimatings (30) (or NEHRP site classes) from Shallow Velocity Models (Depths < 30 m). Bull. Seismol. Soc. Am., 94: 591–597 (**7 pages**).

Chesner, C.A.; Rose, W.I.; Deino, A.L.; Drake, R.; Westgate, J. A., (1991). Eruptive history of Earth's largest Quaternary caldera (Toba, Indonesia) clarified. Geology. 19(3): 200-203 (**4 pages**).

Chesner, C.A.; Luhr, J.F., (2010). A melt inclusion study of the Toba Tuffs, Sumatra, Indonesia. J. Volcanol. Geotherm. Res., 197(1-4): 259-278 (**20 pages)**.

Chesner, C.A., (2012). The Toba caldera complex. Q. Int., 258: 5-18 (**14 pages**).

Chesner, C.A.; Barbee, O.A.; McIntosh, W.C., (2020). The enigmatic origin and emplacement of the Samosir Island lava domes, Toba Caldera, Sumatra, Indonesia. Bull. Volcanol., 82(3): 1-20 (**20 pages**).

Claprood, M.; Asten, M.W.; Kristek, J., (2012). Combining HVSR microtremor observations with the SPAC method for site resonance study of the Tamar Valley in Launceston. Geophys. J. Int., 191(2): 765-780 (**16 pages**).

Daryono, M.R.; Natawidjaja, D.H.; Sieh, K., (2012). Twin-surface ruptures of the March 2007 M> 6 earthquake doublet on the Sumatran Fault. Bull. Seismol. Soc. Am., 102(6): 2356-2367 (**12 pages**).

Forte, G.; Chiocarelli, E.; De Falco, M; Cito, P.; Santo, A.; Lervolino, I., (2019). Seismic soil classification of Italy based on surface geology and shear-wave velocity measurements. Soil Dyn. Earthquake Eng., 122: 79-93 (**15 pages**).

Geethanjali, K.; Achyuthan, H.; Jaiswal, M., (2019). The Toba tephra as a late Quaternary stratigraphic marker: investigations in the Sagileru river basin, Andhra Pradesh, India. Q. Int., 513: 107-123 (**17 pages**).

Goda, K.; Kiota, T.; Fokhrel, R.M.; Chiaro, G.; Katagiri, T.; Sharma, K.; Wilkinson, S., (2015). The 2015 Gorkha Nepal earthquake: Insights from earthquake damage survey. Front. Built Environ., 1(8): (**15 pages**).

Gualandi, A.; Liu, Z.; Rollins, C. (2020). Post-large earthquake seismic activities mediated by aseismic deformation processes. Earth Planet. Sci. Lett., 530: 115870 (**12 pages**).

Hayashi, Y.; Morita, Y. (2003). An image of a magma intrusion process inferred from precise hypocentral migrations of the earthquake swarm east of the Izu Peninsula. Geophys. J. Int., 153(1): 159-174 (**16 pages**).

Horton, S. (2012). Disposal of hydrofracking waste fluid by injection into subsurface aquifers triggers earthquake swarm in central Arkansas with potential for damaging earthquake. Seismol. Res. Lett., 83(2): 250-260 (**11 pages**).

Hurukawa, N.; Wulandari, B. R.; Kasahara, M., (2014). Earthquake history of the Sumatran fault, Indonesia, since 1892, derived from relocation of large earthquakes. Bull. Seismol. Soc. Am., 104(4): 1750-1762 (**13 pages**).

Irwandi, H.; Rosid, M.S.; Mart, T., (2021). The effects of ENSO, climate change and human activities on the water level of Lake Toba, Indonesia: a critical literature review. Geosci. Lett., 8(1): 1-13 (**14 pages**).

Jiang, C.; Yahong, D.; Huangdong, M.; You, X.; Ge, C., (2022). A microtremor study to reveal the dynamic response of earth fissure site: the case study in Fenwei Basins, China. Environ. Earth Sci., 81(3): 1-15 (**15 pages**).

Knight, M.D.; Walker, G.P.; Ellwood, B.B.; Diehl, J.F., (1986). Stratigraphy, paleomagnetism, and magnetic fabric of the Toba Tuffs: constraints on the sources and eruptive styles. J. Geophys. Res.: Solid Earth. 91(B10): 10355-10382 (**28 pages)**.

Koulakov, I.; Yudistira, T.; Luehr, B.G., (2009). P, S velocity and VP/VS ratio beneath the Toba caldera complex (Northern Sumatra) from local earthquake tomography. Geophys. J. Int., 177(3): 1121-1139 (**19 pages)**.

Koulakov, I.; Kasatkina, E.; Shapiro, N.M.; Jaupart, C.; Vasilevsky, A.; El Khrepy, S.; Al-Arifi, N.; Smirnov, S., (2016). The feeder system of the Toba supervolcano from the slab to the shallow reservoir. Nat. Commun., 7(1): 1-12 (**12 pages**).

Manzo, R.; Nardone, L.; Gaudiosi, G.; Martino, C.; Galluzzo, D.; Bianco, F.; Di Maio, R., (2022). A first 3-D shear wave velocity model of the Ischia Island (Italy) by HVSR inversion. Geophys. J. Int., 230(3): 2056-2072 (**17 pages).**

Maresca, R.; Nardone, L.; Gizzi, F. T.; Potenza, M. R., (2018). Ambient noise HVSR measurements in the Avellino historical centre and surrounding area (southern Italy). Correlation with surface geology and damage caused by the 1980 Irpinia-Basilicata earthquake. Measurement. 130: 211–222 (**12 pages**).

Muksin, U.; Bauer, K.; Haberland, C., (2013). Seismic Vp and Vp/Vs structure of the geothermal area around Tarutung (North Sumatra, Indonesia) derived from local earthquake tomography. J. Volcanol. Geotherm. Res., 260: 27-42 (**17 pages**).

Muksin, U.; Haberland, C.; Nukman, M.; Bauer, K.; Weber, M., (2014). Detailed fault structure of the Tarutung Pull-Apart Basin in Sumatra, Indonesia, derived from local earthquake data. J. Asian Earth Sci, 96: 123-131 (**9 pages**).

Muksin, U.; Bauer, K.; Muzli, M.; Ryberg, T.; Nurdin, I.; Masturiyono, M.; Weber, M., (2019). AcehSeis project provides insights into the detailed seismicity distribution and relation to fault structures in Central Aceh, Northern Sumatra. J. Asian Earth Sci., 171: 20–27 (**8 pages**).

Nakamura, Y., (2009)**.** Basic structure of QTS (HVSR) and examples of applications. In increasing seismic safety by combining engineering technologies and seismological data. Springer, Dordrecht. 33–51 (**19 pages**).

Parker, R.N.; Hancox, G.T.; Petley, D.N.; Messey, C.I.; Densmore, A.L.; Rosser, J.N., (2015). Spatial distributions of earthquake-induced landslides and hillslope preconditioning in the northwest South Island, New Zealand. Earth Surf. Dyn., 3(4): 501–525 (**25 pages**).

Pasari, S.; Simanjuntak, A.V.; Mehta, A.; Sharma, Y., (2021). A synoptic view of the natural time distribution and contemporary earthquake hazards in Sumatra, Indonesia. Nat. Hazard., 108(1): 309-321 (**13 pages**).

Pearce, N.J.; Westgate, J.A.; Gualda, G.A.; Gatti, E.; Muhammad, R.F., (2020). Tephra glass chemistry provides storage and discharge details of five magma reservoirs which fed the 75 ka Youngest Toba Tuff eruption, northern Sumatra. J. Quat. Sci., 35(1-2): 256-271 (**16 pages**).

Ryberg, T.; Muksin, U.; Bauer, K., (2016). Ambient seismic noise tomography reveals a hidden caldera and its relation to the Tarutung pull-apart basin at the Sumatran Fault Zone, Indonesia. J. Volcanol. Geotherm. Res., 321: 73-84 (**17 pages**).

Ross, Z.E.; Cochran, E.S., (2021). Evidence for latent crustal fluid injection transients in Southern California from long-duration earthquake swarms. Geophys. Res. Lett., 48(12): e2021GL092465.

Sarma, N.S.; Kiran, R.; Rama Reddy, M.; Iyer, S.D.; Peketi, A.; Borole, D.V.; Krishna, M.S., (2018). Hydrothermal alteration promotes humic acid formation in sediments: a case study of the Central Indian Ocean Basin. J. Geophys. Res.: Oceans, 123(1): 110-130 (**21 pages**).

Seivane, H.; García-Jerez, A.; Navarro, M.; Molina, L.; Navarro-Martínez, F., (2022). On the use of the microtremor HVSR for tracking velocity changes: a case study in Campo de Dalías basin (SE Spain). Geophys. J. Int., 230(1): 542-564 (**23 pages**).

Shelly, D.R.; Hill, D. P.; Massin, F.; Farrell, J., Smith, R.B., Taira, T.A. (2013). A fluid-driven earthquake swarm on the margin of the Yellowstone caldera. J. Geophys. Res. Solid Earth. 118(9): 4872-4886 (**15 pages**).

Sieh, K.; Natawidjaja, D., (2000). Neotectonics of the Sumatran fault, Indonesia. J. Geophys. Res.: Solid Earth, 105(B12): 28295–28326 (**32 pages**).

Soeprobowati, T.R. (2015). Integrated lake basin management for save Indonesian lake movement. Procedia Environ. Sci., 23: 368-374 (**7 pages**).

Stankiewicz, J.; Ryberg, T.; Haberland, C.; Fauzi.; Natawidjaja, D. (2010). Lake Toba volcano magma chamber imaged by ambient seismic noise tomography. Geophys. Res. Lett., 37(17) (**5 pages**).

Stanko, D.; Markušić, S.; Strelec, S.; Gazdek, M. (2017). Equivalent-linear site response analysis on the site of the historical Trakošćan Castle, Croatia, using HVSR method. Environ. Earth Sci., 76(18): 1-21 (**21 pages**).

Tün, M.; Pekkan, E., Ozel, O.; Guney, Y., (2016). An investigation into the bedrock depth in the Eskisehir Quaternary Basin (Turkey) using the microtremor method. Geophys. J. Int., 207(1): 589–607 (**19 pages**).

AUTHOR (S) BIOSKETCHES

Simanjuntak, A.V.H., Ph.D. Candidate, [1]Graduate School of Mathematics and Applied Sciences, Universitas Syiah Kuala, Banda Aceh, Indonesia. [2]Meteorological, Climatological, and Geophysical Agency, BMKG, Banda Aceh, Aceh, Indonesia, Tsunami and Disaster Mitigation Research Center, Universitas Syiah Kuala, Gampong Pie, Indonesia.
- Email: *andrean.simanjuntak@bmkg.go.id*
- ORCID: 0000-0003-0623-0037
- Web of Science ResearcherID: NA
- Scopus Author ID: 57195483722
- Homepage: http://bmkg.go.id/

Muksin, U., Ph.D., Associate Professor, Tsunami and Disaster Mitigation Research Center, Universitas Syiah Kuala, Gampong Pie, Indonesia.
- Email: *muksin.umar@unsyiah.ac.id*
- ORCID: 0000-0001-7297-8065
- Web of Science ResearcherID: W-3934-2018
- Scopus Author ID: 55795600300
- Homepage: http://fsd.unsyiah.ac.id/muksinumar/

Arifullah, A., B.Sc. Master Student, Tsunami and Disaster Mitigation Research Center, Universitas Syiah Kuala, Gampong Pie, Indonesia.
- Email: *arifullah.abd@gmail.com*
- ORCID: 0000-0003-4432-1378
- Web of Science ResearcherID: NA
- Scopus Author ID: NA
- Homepage: http://tdmrc.unsyiah.ac.id/

Lythgoe, K., Ph.D. Presidential Post Doctoral, Earth Observatory of Singapore, Nanyang Techonological of Singapore, Singapore.
- Email: *karen.lythgoe@ntu.edu.sg*
- ORCID: 0000-0002-7642-6900
- Web of Science ResearcherID: NA
- Scopus Author ID: 55927374800
- Homepage: https://www.karenlythgoe.com/

Asnawi, Y., Ph.D. Associate Professor, Universitas Islam Negeri Ar-Raniry, Lorong Ibnu Sina, Syiah Kuala, Kota Banda Aceh, Aceh, Indonesia.
- Email: *yusran@ar-raniry.ac.id*
- ORCID: 0000-0003-0806-1716
- Web of Science ResearcherID: NA
- Scopus Author ID: 57217127838
- Homepage: https://uin.ar-raniry.ac.id/

Sinambela, M., Ph.D., Senior Researcher, Meteorological, Climatological, and Geophysical Agency, BMKG, Medan, Indonesia.
- Email: *marzuki.sinambela@bmkg.go.id*
- ORCID: 0000-0003-3363-4440
- Web of Science ResearcherID: NA
- Scopus Author ID: 57189232496
- Homepage: http://bmkg.go.id/

Rizal, S., Ph.D., Professor, Graduate School of Mathematics and Applied Sciences, Universitas Syiah Kuala, Banda Aceh Indonesia.
- Email: *srizal@unsyiah.ac.id*
- ORCID: 0000-0002-7691-9449
- Web of Science ResearcherID: V-7627-2017
- Scopus Author ID: 56950902200
- Homepage: http://fsd.unsyiah.ac.id/syamsul_rizal/

Wei, S., Ph.D., Professor, [1]Asian School of the Environment, Nanyang Technological University of Singapore. Singapore. [2]Earth Observatory of Singapore, Nanyang Technological of Singapore, Singapore.
- Email: *shjwei@ntu.edu.sg*
- ORCID: 0000-0002-0319-0714
- Web of Science ResearcherID: M-2137-2015
- Scopus Author ID: 25925537600
- Homepage: https://dr.ntu.edu.sg/cris/rp/rp00132

HOW TO CITE THIS ARTICLE

Simanjuntak, A.V.H.; Muksin, U.; Arifullah, A.; Lythgoe, K.; Asnawi, Y.; Sinambela, M.; Rizal, S.; Wei, S., (2023). Environmental vulnerability characteristics in active swarm region. Global J. Environ., Sci. Manage., 9(2): 211-226.

DOI: 10.22034/gjesm.2023.02.03

url: https://www.gjesm.net/article_696623.html